






PeV–EeV Neutrinos from Gamma-Ray Blazars due to Ultrahigh-energy Cosmic-Ray Propagation

Saikat Das¹ , Nayantara Gupta¹ , and Soebur Razzaque² ¹ Astronomy & Astrophysics Group, Raman Research Institute, Bengaluru 560080, Karnataka, India; saikatdas@rri.res.in, nayan@rri.res.in² Centre for Astro-Particle Physics (CAPP) and Department of Physics, University of Johannesburg, PO Box 524, Auckland Park 2006, South Africa
srazzaque@uj.ac.za

Received 2020 December 30; revised 2021 February 8; accepted 2021 February 8; published 2021 April 1

Abstract

Blazars are potential sources of cosmic-ray acceleration up to ultrahigh energies ($E \gtrsim 10^{18}$ eV). For an efficient cosmic-ray injection from blazars, $p\gamma$ collisions with extragalactic background light (EBL) and cosmic microwave background (CMB) can produce neutrino spectra with peaks near to PeV and EeV energies, respectively. In this work, we analyze the contribution of these neutrinos to the diffuse background measured by the IceCube neutrino observatory. The fraction of neutrino luminosity originating from individual redshift ranges is calculated using the distribution of BL Lacs and FSRQs provided in the Fermi-LAT 4LAC catalog. Furthermore, we use a luminosity-dependent density evolution to find the neutrino flux of unresolved blazars. The results obtained in our model indicate that as much as $\approx 10\%$ of the flux upper bound at a few PeV energies can arise from cosmic-ray interactions with EBL. The same interactions will also produce secondary electrons and photons, initiating electromagnetic cascades. The resultant photon spectrum is limited by the isotropic diffuse γ -ray flux measured between 100 MeV and 820 GeV. The latter, together with the observed cosmic-ray flux at $E > 10^{16.5}$ eV, can constrain the baryonic loading factor, depending on the maximum cosmic-ray acceleration energy.

Unified Astronomy Thesaurus concepts: [High-energy astrophysics \(739\)](#); [Blazars \(164\)](#); [Relativistic jets \(1390\)](#); [Gamma-rays \(637\)](#); [Neutrino astronomy \(1100\)](#); [High-energy cosmic radiation \(731\)](#)

1. Introduction

The IceCube neutrino observatory in Antarctica has been detecting neutrino events between 100 GeV and a few PeV for the last ten years. The existence of a diffuse flux of astrophysical neutrinos (from ~ 10 TeV to a few PeV) has been established, with more than 5σ significance (IceCube Collaboration et al. 2013, 2014), which is inconsistent with an atmospheric origin. The flux is isotropic across the entire sky and in all flavors, indicating that the candidate sources are extragalactic. However, a non-negligible Galactic component may also be present (Razzaque 2013; Ahlers & Murase 2014; Taylor et al. 2014; Neronov et al. 2014; IceCube Collaboration et al. 2017a). The observed all-flavor spectrum can be explained by a single power law, with a best-fit spectral index of $2.89^{+0.2}_{-0.19}$ (Aartsen et al. 2015; Schneider 2019). While γ -rays can be produced in both leptonic and hadronic processes, neutrinos are an exclusive probe of hadronic interactions. They point back to their sources, and are important messengers of cosmic-ray acceleration. IceCube has a real-time alert program that selects high-energy muon neutrino events ($\gtrsim 100$ TeV) for the rapid detection of electromagnetic counterparts arriving from the same direction (IceCube Collaboration et al. 2017b). The IceCube-170922A alert led to the 3σ association of a flaring γ -ray blazar, TXS 0506+056, in spatial and temporal coincidence with a ~ 0.3 PeV muon track (IceCube Collaboration et al. 2018a, 2018b). Other, less significant, candidate events with blazar-neutrino spatial coincidence have also been subsequently identified (Steehgs et al. 2019; Garrappa et al. 2019; Franckowiak et al. 2020a).

Blazars are a subclass of radio-loud AGNs, whose jet emission is closely aligned along the observer’s line of sight. Blazars are further classified as FSRQs and BL Lacs, depending on the prominence of emission lines in the observed

spectral-energy distribution (SED). They have been long considered as the sources of high-energy neutrinos (Eichler 1979; Sikora et al. 1987; Berezhinskii & Ginzburg 1981; Stecker et al. 1991; Mannheim et al. 1992; Szabo & Protheroe 1994; Atoyan & Dermer 2001; Becker 2008; Murase et al. 2014; Petropoulou et al. 2015; Palladino et al. 2019; Yuan et al. 2020; Rodrigues et al. 2020). Once accelerated inside the jet, the electrons and positrons lose energy via synchrotron emission and inverse-Compton (IC) scattering. Cosmic rays can interact with ambient matter (pp collision) or radiation ($p\gamma$ process) to produce charged and neutral pions, which decay to produce γ rays and neutrinos. The target photons for the $p\gamma$ process are provided by synchrotron/IC photons, or external photons from the broad-line region (BLR), accretion disk (AD), or dusty torus (DT). Despite the plausible association of blazars with neutrinos observed in a few cases, it is difficult to explain the observed neutrino spectrum based on blazars alone. Using the Fermi-LAT 2LAC catalog to define its search positions, the IceCube collaboration has shown that astrophysical neutrinos from blazars can only account for $\sim 7\%$ – 27% of the observed flux between 10 TeV and 2 PeV. The limit depends on various weighting schemes’ accounting for the relative neutrino flux from a specific source (IceCube Collaboration et al. 2017c). Thus, the origin of these neutrinos is still controversial.

Cosmic rays can also escape their sources without undergoing internal $p\gamma$ interactions. Ultrahigh-energy cosmic rays (UHECRs; $E \gtrsim 10^{18}$ eV), with energies greater than the threshold of photopion production on CMB ($E_{\text{th}}^{p,\pi} \approx 6 \cdot 10^{19}$ eV), can yield EeV neutrinos. In this work, we investigate the neutrino flux produced by cosmic rays that escape from the blazar emission region and interact with the EBL, comprising of UV/optical/IR photons, as well as the radio photons of the CMB. The threshold for photopion production on EBL peaks at $E_{\text{th}}^{p,\pi} \approx 10^{17}$ eV, resulting in most neutrino events occurring in a range from

a few PeV to tens of PeV. The exact value of the peak energy, and the width of the spectrum, depend on the injection spectrum and $E_{p,\max}$. It has been shown, using AGN-source density evolution, derived from X-ray luminosities, that neutrinos resulting from such a process can account for the PeV neutrino flux measured by IceCube (Kalashev et al. 2013). An angular correlation of these neutrino events with the blazar population is difficult to obtain, since cosmic rays are deflected from the source direction by an extragalactic magnetic field (EGMF). The lepto-hadronic SED modeling of blazars reveals that protons can be accelerated up to ultrahigh energies in the comoving jet frame. Their escape depends on the seed photon density of $p\gamma$ interactions inside the AGN jet (Mastichiadis 1996; Murase et al. 2012; Razaque et al. 2012; Böttcher et al. 2013; Tavecchio 2014; Xue et al. 2019; Sahu et al. 2019; Das et al. 2020).

The 8 yr Fermi-LAT 4LAC catalog contains 80% more sources, as compared to the previous 3LAC catalog (Ackermann et al. 2015a; Ajello et al. 2020). The following analysis investigates the cumulative neutrino spectrum from 4LAC blazars, resulting in the aforementioned process. Furthermore, we use the known luminosity function of BL Lacs and FSRQs to extrapolate the sources below the Fermi-LAT sensitivity, and include the contribution from these unresolved sources (Ajello et al. 2012, 2013). The injected cosmic-ray luminosity is assumed to be proportional to the observed point-source γ -ray luminosity by a constant factor. The electrons and photons, simultaneously produced with neutrinos, undergo electromagnetic cascade to produce γ -rays. Its contribution to the isotropic diffuse γ -ray background (IGRB), measured by Fermi-LAT between 100 MeV and 820 GeV, is also calculated (Ackermann et al. 2015b). We do not prefer any cosmic-ray acceleration mechanism over others proposed hitherto for this scenario. In Section 2, we summarize the basic methodology of neutrino flux calculations, and present our results for various source parameters. We discuss the implications of our work in Section 3, and draw our conclusions in Section 4.

2. Results

2.1. Cosmic-Ray Injection and Propagation

The integrated γ -ray flux, between 100 MeV and 100 GeV, observed from the direction of resolved blazars is reported in the 4LAC catalog by the quantity F_{100} , in units of $\text{erg cm}^{-2} \text{s}^{-1}$. We represent the K-corrected γ -ray luminosity values corresponding to this flux, and the redshift of the sources, by L_{100} . Thus we have

$$\begin{aligned} F_{100} &= \int_{100 \text{ MeV}}^{100 \text{ GeV}} \epsilon_\gamma \frac{dN}{d\epsilon_\gamma} d\epsilon_\gamma \\ L_{100} &= 4\pi d_L^2 F_{100} (1+z)^{\Gamma-2} \end{aligned} \quad (1)$$

where z is the redshift of the source, d_L is the luminosity distance, and Γ is the slope of the observed γ -ray spectrum. The γ -ray luminosity inside the source, L'_{100} , is usually smaller than the observed luminosity, L_{100} , due to relativistic beaming. The intrinsic γ -ray luminosity in the comoving frame of the jet is Doppler-boosted by the factor $L_{100} = (\delta_e^6/\Gamma_e^2)L'_{100}$ for FSRQs, and $L_{100} = \delta_e^4 L'_{100}$ for BL Lacerate objects (Dermer & Menon 2009). Here, δ_e and Γ_e denote the Doppler factor and bulk Lorentz factor of the emitting region in the relativistic jet. We define the baryonic loading factor, η , to be a constant, for

all blazars, connecting the intrinsic kinetic power, L'_p , in cosmic rays with the intrinsic γ -ray luminosity, L'_{100} .

$$L'_p = \eta L'_{100} \quad (2)$$

The emission region of the jet contains both leptons and hadrons. We assume that the observed γ -ray flux, F_{100} , originates only from leptonic processes inside the source, and baryons carry far more energy than leptons. For the analysis presented in this paper, we consider only those protons with $E > 10$ PeV injected as cosmic rays. As such, the cosmic-ray luminosity outside the jet (AGN frame) transforms as $L_p = \Gamma_e^2 L'_p$ (Celotti & Ghisellini 2008). Hence, in the observer frame, the scaling between the injected cosmic-ray luminosity (L_p) and the resulting observed γ -ray luminosity (L_{100}) is given as

$$\begin{aligned} L_p &= \Gamma_e^2 L'_p = \Gamma_e^2 \eta L'_{100} \\ &\simeq \eta L_{100} / \Gamma_e^2 = \eta_{\text{eff}} L_{100} \end{aligned} \quad (3)$$

where we assume that $\delta_e \simeq \Gamma_e$, for jet opening angles $\theta_j \sim 1/\Gamma_e$, and that $\eta_{\text{eff}} = \eta/\Gamma_e^2$ is the effective baryonic loading.

Once injected into extragalactic space, the cosmic rays propagate, and undergo $p\gamma$ interactions with EBL and CMB photons to produce charged and neutral pions ($p + \gamma_{\text{bg}} \rightarrow p\pi^0$, or $n\pi^+$). The decay of π^+ and π^0 results in neutrinos and γ -rays, respectively. Including Bethe–Heitler pair-production interactions ($p + \gamma_{\text{bg}} \rightarrow e^+e^-$), the secondary e^\pm and γ -rays initiate electromagnetic (EM) cascades down to GeV energies. The high-energy photons undergo pair-production processes, while the e^\pm can undergo triplet pair-production, synchrotron, and IC processes, upscattering the background photons to higher energies. The resulting photon spectrum peaks at \sim TeV energies, thereby contributing to the IGRB flux measured by Fermi-LAT (Ackermann et al. 2015b). The neutrinos propagate unhindered by interactions, and undeflected by cosmic magnetic fields, to reach the observer, and contribute to the isotropic diffuse neutrino background at PeV energies.

Cosmic rays injected from the blazars are propagated using the CRPROPA 3 simulation framework to obtain the neutrino, γ -ray and cosmic-ray flux measurements at Earth (Alves Batista et al. 2016). We consider an injection spectrum of the shape $dN/dE \propto E^{-\alpha_p}$. CRPROPA 3 allows us to include all energy-loss processes, and also takes into account the adiabatic expansion of the universe. Since we are interested in diffuse fluxes, a null magnetic field is considered for CR propagation. The propagation of secondary EM particles, initiating the electromagnetic cascade, is solved using DINT code (Lee 1998; Heiter et al. 2018). The EM cascade of secondary e^\pm and γ photons depends on the pervading magnetic field, and we set the rms field strength $B_{\text{rms}} = 0.1$ nG for the EGMF. We use the EBL model of Gilmore et al. (2012) for both cosmic-ray interactions and EM cascade.

The efficiency of neutrino production by cosmic rays will depend on the number of interaction lengths, and thus on the redshift, of their sources. We assume that cosmic rays are injected from 10 PeV up to a maximum energy, $E_{p,\max}$. The fraction of injected cosmic-ray energy (\mathcal{E}_p), from a redshift z , carried away by cascade photons (\mathcal{E}_γ) and secondary neutrinos

Table 1
Parameter Values for the Best-fit LDDE Model

Sample	A [Gpc ⁻³]	$L_*/10^{48}$ [erg s ⁻¹]	γ_1	γ_2	z_c^*	α	p_1^*	p_2	μ	σ
BL Lac	$3.39^{+7.44}_{-2.13}$	$0.28^{+0.43}_{-0.21}$	$0.27^{+0.26}_{-0.46}$	$1.86^{+0.86}_{-0.48}$	$1.34^{+0.22}_{-0.27}$	$0.0453^{+0.0498}_{-0.0652}$	$2.24^{+1.07}_{-1.25}$	$-7.37^{+2.95}_{-5.43}$	$2.10^{+0.03}_{-0.03}$	$0.26^{+0.02}_{-0.02}$
FSRQ	$3.06^{+0.23}_{-0.23}$	$0.84^{+0.49}_{-0.49}$	$0.21^{+0.12}_{-0.12}$	$1.58^{+0.27}_{-0.27}$	$1.47^{+0.16}_{-0.16}$	$0.21^{+0.03}_{-0.03}$	$7.35^{+1.74}_{-1.74}$	$-6.51^{+1.97}_{-1.97}$	$2.44^{+0.01}_{-0.01}$	$0.18^{+0.01}_{-0.01}$

(\mathcal{E}_ν), are given by $f_\nu(z)$ and $f_\gamma(z)$, respectively.

$$f_\nu = \frac{\mathcal{E}_\nu(z)}{\mathcal{E}_p} = \frac{1}{\mathcal{E}_p} \times \int_{10\text{TeV}}^{E_{p,\text{max}}} \epsilon_\nu (dN/d\epsilon_\nu) d\epsilon_\nu \quad (4)$$

$$f_\gamma = \frac{\mathcal{E}_\gamma(z)}{\mathcal{E}_p} = \frac{1}{\mathcal{E}_p} \times \int_{10\text{MeV}}^{E_{p,\text{max}}} \epsilon_\gamma (dN/d\epsilon_\gamma) d\epsilon_\gamma \quad (5)$$

All quantities in the above equations are calculated in the observer frame, using one-dimensional simulations in CRPROPA 3, for a fixed α_p , and different source distances. The value of \mathcal{E}_p is fixed at all redshifts. These quantities signify the energy-loss fraction of protons in various secondary channels; hence, a null intergalactic magnetic field is assumed. The latter can eventually deflect the parent cosmic rays, smeared over a solid angle, Ω , thereby resulting in a diffuse secondary flux. The normalization to the neutrino luminosity from a blazar at redshift z , and γ -ray luminosity, L_{100} is thus obtained by the following condition (using Equation (3)):

$$L_\nu^{\text{obs}} = f_\nu L_p = f_\nu \eta_{\text{eff}} L_{100} \quad (6)$$

The same expression also holds for secondary photon luminosity, L_γ^{obs} , with f_ν replaced by f_γ . Summing over all sources at all redshifts and different directions, the cumulative diffuse neutrino spectrum at Earth is

$$F_\nu^{\text{tot}} = \frac{1}{\Omega} \sum_i \left(\frac{L_\nu^{\text{obs}}}{\Omega d_L^2} \right) \quad [\text{erg cm}^{-2}\text{s}^{-1}\text{sr}^{-1}] \quad (7)$$

where d_L is the luminosity distance, corresponding to redshift z . The summation i runs over the number of blazars in the sample space. We consider a conservative upper limit, $\Omega = 4\pi$, which gives the minimum flux possible in this scenario.

2.2. Blazar Luminosity Distribution

The fourth catalog of Fermi-LAT AGNs, detected over the period between 2008 August to 2016 August at high Galactic latitudes, $|b| > 10^\circ$, contains 2863 objects in the energy range, between 50 MeV and 1 TeV. This paper uses the sources from the latest 4LAC catalog to calculate the cumulative neutrino and cascade gamma-ray fluxes from blazars, originating from cosmic-ray interactions during extragalactic propagation. There are a total of 655 FSRQs and 1067 BL Lacs listed in the entire catalog. The redshift information is available for all FSRQs but, is lacking for 36% of the BL Lacs. Moreover, there are 1077 blazar candidates of unknown type (BCU). The number density of blazars depends on both luminosity and redshift distributions. The luminosity function (LF) is modeled as a double power law, multiplied by the photon-index evolution. We use the parameterization of Ajello et al. (2012, 2013) to evaluate the distribution of BL Lac objects and FSRQs, including unresolved sources. At $z=0$, the number of sources, N , per

comoving volume, V_c , emitted luminosity, L_{100} , between 0.1 – 100 GeV, and the slope of γ -ray flux, Γ , is expressed as

$$\Phi(L_{100}, z=0, \Gamma) = \frac{dN}{dL_{100} dV_c d\Gamma} = \frac{A}{\ln(10) L_{100}} \times \left[\left(\frac{L_{100}}{L_*} \right)^{\gamma_1} + \left(\frac{L_{100}}{L_*} \right)^{\gamma_2} \right]^{-1} g(\Gamma, L_{100}) \quad (8)$$

The photon-index distribution, $g(\Gamma, L_{100})$, is considered to be Gaussian, with the mean and dispersion given by μ and σ , respectively, as

$$g(\Gamma, L_{100}) = \exp \left[-\frac{[\Gamma - \mu(L_{100})]^2}{2\sigma^2} \right] \quad (9)$$

The mean is parametrized as a function of luminosity,

$$\mu(L_{100}) = \mu^* + \beta \times [\log(L_{100}) - 46] \quad (10)$$

The redshift evolution is incorporated by the factor $e(z, L_{100})$, such that the luminosity-dependent density evolution (LDDE) is represented as

$$\Phi(L_{100}, z, \Gamma) = \Phi(L_{100}, z=0, \Gamma) \times e(z, L_{100}) \quad (11)$$

The evolutionary factor is expanded as

$$e(z, L_{100}) = \left[\left(\frac{1+z}{1+z_c(L_{100})} \right)^{-p_1(L_{100})} + \left(\frac{1+z}{1+z_c(L_{100})} \right)^{-p_2} \right]^{-1} \quad (12)$$

with the following parameterizations,

$$\begin{aligned} z_c(L_{100}) &= z_c^*(L_{100}/10^{48})^\alpha \\ p_1(L_{100}) &= p_1^* + \tau \times [\log(L_{100}) - 46] \end{aligned} \quad (13)$$

where z_c is the redshift at which the evolution changes sign from positive to negative, and z_c^* is the redshift peak for a luminosity of 10^{48} erg s⁻¹. We use the values of the 12 parameters ($A, \gamma_1, \gamma_2, L_*, z_c^*, \alpha, p_1^*, p_2, \mu, \sigma, \beta, \tau$) as obtained for the best-fit LDDE model, reported in Ajello et al. (2012, 2013). The wrong positive sign of p_1 and p_2 in earlier work has been corrected in Ajello et al. (2015). We list the values in Table 1. For BL Lacs, $\beta = 0.0646^{+0.0234}_{-0.0207}$ and $\tau = 4.92^{+1.45}_{-2.12}$, and for FSRQs, they are zero. Integrating $\Phi(L_{100}, z, \Gamma)$ gives the total number of sources, both resolved and unresolved, combined together. We follow the method of Palladino et al. (2019) (their Appendix B), and write the number density in terms of

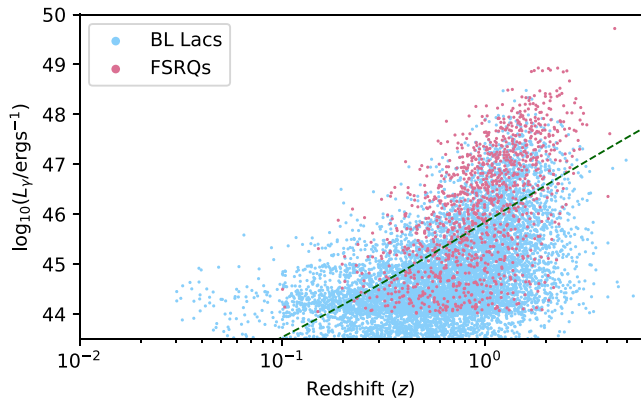


Figure 1. Distribution of blazars in luminosity-redshift space, based on the luminosity function deduced in Ajello et al. (2012, 2013). The dashed line separates the region into resolved and unresolved sources in the Fermi-LAT survey.

redshift, z , and $\ell = \log_{10}(L_{100}/\text{erg s}^{-1})$,

$$\frac{dN}{dzd\ell d\Gamma} = \frac{dV_c}{dz} \times \frac{dL_{100}}{d\ell} \times \frac{dN}{dL_{100}dV_c d\Gamma} \quad (14)$$

To calculate the flux from a complete sample, we integrate Equation (11) over suitable ranges of luminosity, spectral index, and redshift. For FSRQs, $\ell \in [44.0, 52.0]$, $\Gamma \in [1.8, 3.0]$, and $z \in [0.01, 6.0]$. The range of values for BL Lacs are $\ell \in [43.85, 52]$, $\Gamma \in [1.45, 2.80]$, and $z \in [0.03, 6.0]$. A total of 9172 blazars are obtained by integrating over the entire parameter range given in Equation (14). A representative distribution of blazars in the $\ell - z$ space is shown in Figure 1. The dashed line corresponds to a flux of $\phi_\gamma = 1.25 \times 10^{-12} \text{ erg cm}^{-2} \text{ s}^{-1}$ and $\Gamma = 2$, roughly separating the region into resolved and unresolved sources above and below, respectively. This threshold flux is chosen to match the 4LAC statistics of ~ 2800 observed blazars, including 1077 blazars of unknown type. Thus, Figure 1 corresponds to 2072 resolved, and 5931 unresolved BL Lac objects, while there are 742 resolved, and 427 unresolved FSRQs. The low-luminosity BL Lac objects ($L_{100} < 10^{44} \text{ erg s}^{-1}$) show a negative redshift evolution, and are mostly confined at low redshifts (Ajello et al. 2013). High luminosities and redshifts are dominated by FSRQs, as expected.

2.3. Secondary Neutrino and γ -Ray Flux

The maximum acceleration energy of a blazar, $E_{p,\text{max}}$, is determined by the escape timescale (t_{esc}), acceleration timescale (t_{acc}), and photohadronic interaction timescales ($t_{p\gamma}$) inside the jet. Having fitted the synchrotron and IC peak with the leptonic component, the SED modeling of representative BL Lac objects shows that the maximum acceleration energy of protons can extend up to 10^{19} eV (Murase et al. 2012; Razzaque et al. 2012; Böttcher et al. 2013; Xue et al. 2019; Sahu et al. 2019; Das et al. 2020). For FSRQs, we have used the values of δ_e , Γ_e , and seed photon density as obtained in the modeling of CTA 102 (Prince et al. 2018), finding that acceleration dominates up to a few times 10^{19} eV . This has also been noted in relation to a more generic class of quasar-hosted blazars in Murase et al. (2014). In the following analysis, we consider optimistic values of $E_{p,\text{max}}$, based on these results.

2.3.1. Contributions from Resolved γ -Ray Blazars

We first calculate the γ -ray and neutrino flux from Fermi-LAT resolved sources (BL Lacs + FSRQs). For simplicity, we assume that the sources inject only protons as cosmic rays between 10 PeV and 1 EeV, and fix the injection spectral index to $\alpha_p = 2.6$. The effects of variation of these parameters will be discussed below. For this case, we consider that the value of the baryonic loading factor $\eta_{\text{eff}} = 10$. Sources lacking redshift information are excluded from our analysis. This leaves out 381 BL Lac objects across the entire catalog. The sources are binned in a two-dimensional (ℓ, z) grid, where $\ell = \log_{10}(L_{100}/\text{erg s}^{-1})$. We take the step sizes $\Delta\ell = 0.5$ over the range 43.5 to 52.0, and $\Delta z = 0.1$ over the range 0.0–6.0, which covers the entire 4LAC catalog. The mean values, ℓ_m and z_m , for a given bin are used to obtain the secondary neutrino and γ -ray flux, in accordance with Equation (7). The number of sources, w , in a grid provides the weight factor to the normalization of secondary fluxes. The resulting γ -ray and neutrino fluxes are shown in the left panel of Figure 2. The neutrino spectrum peaks at an energy of $E_\nu \approx 6 \text{ PeV}$. At around 6.3 PeV, $\bar{\nu}_e$ have an increased probability of interaction with ice to produce the on-shell W^- boson, due to Glashow resonance (GR). However, it is challenging to detect the GR signal (Biehl et al. 2017; Huang & Liu 2020). The enhancement in the number of events due to GR is not substantial in the relevant energy range, as predicted by Bhattacharya et al. (2011), who also proposed to use it as a discriminator between the $p\gamma$ and pp origin of neutrinos. Based on the current event statistics, and taking into account that no GR neutrinos are detected, this also indicates that the IceCube high-energy neutrinos originate predominantly from $p\gamma$, rather than pp processes (Sahu & Zhang 2018). Our calculated flux is an order of magnitude lower than the IceCube upper limit at this energy. The peak value is also comparable to the projected three-year sensitivity of the POEMMA detector. The contribution to this neutrino flux from each redshift bin will depend on the number of blazars, and their luminosity values in that bin. The right panel of Figure 2 shows the fraction of neutrino luminosity, for each redshift bin individually, for BL Lacs and FSRQs. The flux contribution from BL Lacs is approximately constant up to $z = 1$, then falls off sharply for higher z , whereas the emission from FSRQs shows a peak near a redshift value of $z = 1$.

2.3.2. Contributions from Resolved and Unresolved γ -Ray Blazars

Here, we show the secondary fluxes, corresponding to the distribution obtained from the luminosity function, in the left panel of Figure 3. The number of blazars, w , in each of the (ℓ, z) grid is calculated for the same values of $\Delta\ell$ and Δz used in the preceding case. The dotted, dashed, and solid curves indicate the fluxes for the maximum permitted values of η_{eff} , corresponding to each value of $E_{p,\text{max}}$. The latter is derived from the UHECR flux as measured by the Pierre Auger Observatory (PAO) (The Pierre Auger Collaboration et al. 2019), which imposes an upper bound of $\eta_{\text{eff}} = 11.1, 5.8,$ and 4.4 , for $E_{p,\text{max}} = 1, 10,$ and 100 EeV , respectively. This is shown in the right panel of Figure 3. We see that cosmic-ray interactions can explain a little over 10% of the IceCube flux upper limit at $\sim 6 \text{ PeV}$. For $E_{p,\text{max}} = 1$ and 10 EeV , POEMMA should be able to constrain the fluxes after a few years of observation. An increase in the value of $E_{p,\text{max}}$ to 10 EeV increases the cascade photon flux, and saturates the IGRB

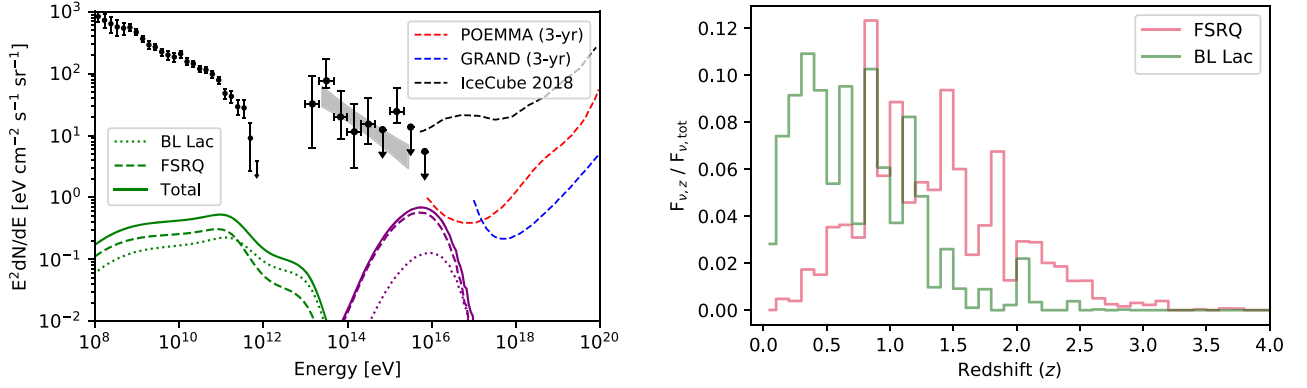


Figure 2. Left: neutrino and IGRB flux from Fermi-detected blazars for $\eta_{\text{eff}} = 10.0$, and $E_{p,\text{max}} = 1$ EeV. Right: fractional contribution to the neutrino flux from each redshift bin, relative to the individual flux from BL Lacs and FSRQs.

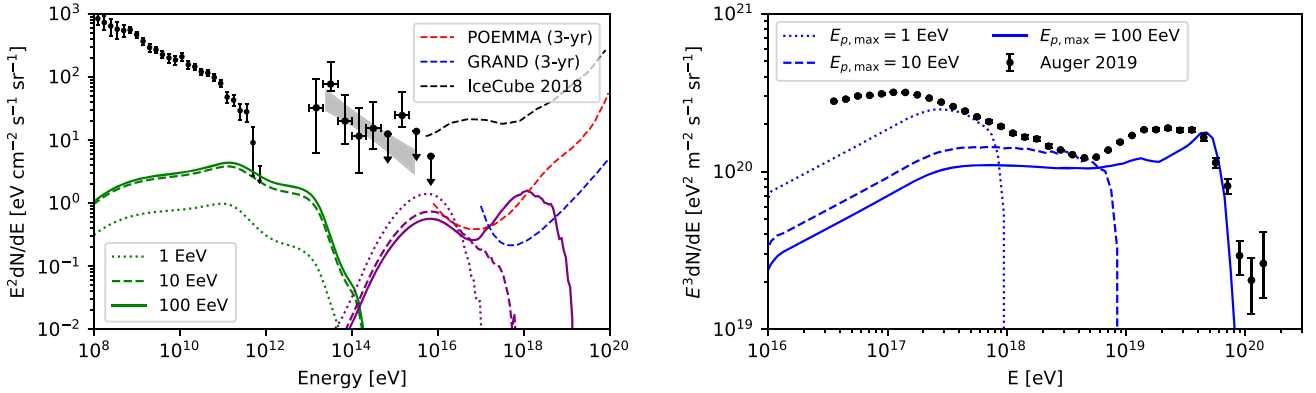


Figure 3. Left: neutrino and IGRB flux, including unresolved blazars, for the maximum values of η_{eff} , corresponding to $E_{p,\text{max}} = 1, 10, \text{ and } 100$ EeV. Right: the observed cosmic-ray spectrum at Earth for the maximum values of η_{eff} , corresponding to $E_{p,\text{max}} = 1, 10, \text{ and } 100$ EeV, such that the UHECR flux is not violated.

background at TeV energies. The neutrino spectrum is broadened for higher $E_{p,\text{max}}$, due to neutrinos arising from photopion interactions with the high-energy tail of the CMB spectrum. With a further increase in $E_{p,\text{max}}$ to 100 EeV, the GZK neutrinos become more prominent, and the neutrino spectrum attains a double-humped shape, characteristic of cosmogenic neutrinos.

The Fermi-LAT IGRB intensity with decrease as fainter sources are resolved by future deep surveys. However, the component deduced in this work is purely diffuse, if the γ -rays from cosmic-ray interactions are not produced along the blazar’s line of sight. To maintain the constraints imposed by the IGRB measurements, the baryonic loading factor, η , must be decreased for $E_{p,\text{max}} \gtrsim 10^{19}$ eV. However, that in turn further decreases the neutrino flux at a few PeV energies. The maximum luminosity in the 4LAC catalog occurs for an FSRQ with $\ell = 48.8$, and $z = 2.534$. The value of $\eta_{\text{eff}} = 11.1$ obtained for $E_{p,\text{max}} = 1$ EeV, and bounded by the UHECR data, corresponds to $L_p \sim 6 \cdot 10^{49}$ erg s $^{-1}$ for the most luminous object. The neutrino flux obtained from an individual source, is $F_\nu \propto \eta_{\text{eff}} \propto \eta / \delta_e^2$, for a given value of L_{100} and $E_{p,\text{max}}$. To obtain the same neutrino luminosity for a lower value of η , the value of δ_e must also decrease. Indeed, the value of the Doppler factor may vary for individual AGNs, depending on the accretion rate of the central black hole. It is not possible, however, to extract the Doppler factor and the Lorentz factor of all the individual blazars used in this study based on observations. We therefore make the simplifying assumption, $\delta_e \simeq \Gamma_e$, for the special case of $\theta \sim 1/\Gamma_e$. The maximum value

of the Doppler factor can be $2\Gamma_e$, in which case the required luminosity in injected protons (L_p) is four times lower.

3. Discussions

In this work, we apply a multi-messenger approach to constrain the diffuse flux of PeV–EeV neutrinos originating from cosmic-ray interactions with EBL and CMB. We consider blazars as the candidate source class, injecting cosmic rays up to 1–100 EeV, with a luminosity-dependent injection power, i.e., $L_p \propto L_{100}$ (Padovani et al. 2015). This ensures that more luminous sources contribute more to neutrino and IGRB backgrounds. If the protons are cooled sufficiently inside the jet, they produce neutrino fluxes, depending on the luminosity of target photons via $p\gamma$ interactions (Murase et al. 2014; Tavecchio et al. 2014; Palladino et al. 2019). In contrast, we explicitly assume that the cosmic rays efficiently escape the system. This is justified, as long as the escape rate is higher than the cooling rate of the protons, and acceleration dominates up to the desired $E_{p,\text{max}}$. Our model does not account for the sub-PeV neutrinos, which are expected to be dominated by the neutrinos produced inside high-energy sources. Similar results have been obtained using a likelihood analysis of the IceCube data in Kochocki et al. (2020), where the authors propose that interactions of cosmic rays from blazar AGNs can make up for 30%–40% of the diffuse flux.

A strict L_p/L_{100} correlation may not hold invariably for all sources. The “blazar sequence” predicts that BL Lacs with synchrotron and IC peak at higher energies are fainter in terms

of photon flux (Fossati et al. 1998; Ghisellini & Tavecchio 2008; Ghisellini et al. 2017). Low-luminosity counterparts may be more hadronically powered (higher η_{eff}), since the predicted SED peak energies are higher. Future observation of the γ -ray SED of such sources may provide further information. Here, we find that, for maximum proton acceleration energy, $E_{p,\text{max}}$, between 1 EeV and 100 EeV, the value of η_{eff} ranges from 11.1 to 4.4.

The 4LAC catalog provides redshift information for all of the resolved FSRQs, and most of the BL Lac objects. The deduced luminosity function of BL Lacs indicates that nearly $\sim 65\%$ are yet to be identified. A majority of these are low-luminosity ($L_{\gamma} < 10^{44}$ erg s^{-1}) counterparts, and exhibit a negative redshift evolution. They are modeled as potential UHECR accelerators, owing to the preference of a softer spectral index, consistent with the Fermi acceleration model, as compared to the hard injection required for a flat or positive redshift evolution (Taylor et al. 2015). By including the unresolved sources, the neutrino flux increases by a factor of two at a few PeV. We can therefore state that Fermi-LAT has already detected a significant fraction of the AGNs contributing to the neutrino flux at this energy, particularly the most luminous variety.

Hadronic emission processes can also model GeV–TeV γ -rays from BL Lacs and FSRQs (Böttcher et al. 2013; Petropoulou et al. 2015; Sahu et al. 2019). Leptonic emission alone can also explain the SED up to TeV energies, with neutrinos originating from a radiatively subdominant hadronic component (Keivani et al. 2018). This is applicable to the 3σ association of IceCube-170922A with the blazar TXS 0506+056, while alternate explanations involving the pp process (Banik & Bhadra 2019) or multi-zone emission also exist (Xue et al. 2019, 2021). Recently, the IceCube-200107A event has been correlated with flaring blazar 3HSP J095507.9+355101 (Giommi et al. 2020), and IC190730A has been correlated with PKS 1502+106 (Franckowiak et al. 2020b). However, a correlation of any neutrino event with nearby flaring blazars, such as MrK 421, or Mrk 501 has not been found. This may be due to a low neutrino flux level, resulting from lower cosmic-ray power. The deflection of 10 EeV UHECR protons from these sources at a distance of ≈ 150 Mpc, in 0.1 nG magnetic field, could be $\sim 1^\circ$ for a turbulence correlation length of 1 Mpc. Future detection of neutrinos and cosmic rays in spatial and temporal coincidence with nearby blazars will place our proposition concerning UHECR acceleration onto firmer ground.

The values of $E_{p,\text{max}}$ considered in this study resemble the typical values obtained in the lepto-hadronic/hadronic modeling of blazar SEDs (Mücke et al. 2003; Böttcher et al. 2013). We see that beyond a maximum acceleration energy of ≈ 10 EeV, the IGRB flux is saturated at TeV energies, and so requiring a lower baryon load, which in turn reduces the neutrino flux at a few PeV. Assuming a rigidity-dependent steepening of the cosmic-ray spectrum, the knee for heavier primaries occurs at $E \approx 10^{16.92}$ eV (KASCADE–Grande Collaboration et al. 2011, 2013), beyond which the proton abundance predominates, at least up to $10^{18.2}$ eV. Our choice of injection spectral index $\alpha_p = 2.6$ conforms with that considered in earlier studies for the extragalactic light component in this energy range (Aloisio et al. 2014; Liu et al. 2016).

Our analysis considers protons injected with a minimum energy of 10 PeV. In principle, protons of even lower energy

can also escape, as we assume that the observed γ -rays from these blazars originate solely from leptonic processes. This will increase the luminosity budget. However, a break in the proton spectrum near to 10 PeV may also exist, preferring a harder spectral index below ($\alpha_p < 2$), and thereby reducing the luminosity requirement. Depending on the normalization and the total number of blazars obtained in more updated luminosity-dependent density evolution functions (see, e.g., Qu et al. 2019), the estimates obtained here may change moderately. We do not explore the possible variation in our results due to different parameters of EM cascade, such as extragalactic magnetic fields, EBL models, etc. Earlier studies have shown that these effects are rather moderate (Alves Batista et al. 2015). However, we consider a discrete scenario, with an exemplary choice of parameters, which allows us to adequately explore cosmic-ray interactions with EBL in the context of a diffuse PeV neutrino background.

4. Conclusions

We found that the resolved gamma-ray blazars from the Fermi-4LAC catalog can explain up to 10% of IceCube’s diffuse neutrino flux upper limits at a few PeV energies. This requires a baryon load (cosmic-ray to gamma-ray luminosities) of ≈ 10 . FSRQs are the predominant contributors to the neutrino flux. By including unresolved gamma-ray blazars, the contribution may increase by a factor of two, depending on the maximum injected cosmic-ray energy. The baryon load in this case is bounded by the UHECR flux, and varies between 4 and 11. The gamma-ray flux contribution from UHECR interactions, is constrained by the Fermi diffuse flux upper limit at 820 GeV, depending upon the maximum injected cosmic-ray energy.

Software: CRPROPA 3 (Alves Batista et al. 2016), DINT (Lee 1998; Heiter et al. 2018).

ORCID iDs

Saikat Das  <https://orcid.org/0000-0001-5796-225X>
 Nayantara Gupta  <https://orcid.org/0000-0002-1188-7503>
 Soebur Razzaque  <https://orcid.org/0000-0002-0130-2460>

References

- Aartsen, M. G., et al. 2015, *ApJ*, 809, 98
 Ackermann, M., Ajello, M., Atwood, W. B., et al. 2015a, *ApJ*, 810, 14
 Ackermann, M., Ajello, M., Albert, A., et al. 2015b, *ApJ*, 799, 86
 Ahlers, M., & Murase, K. 2014, *PhRvD*, 90, 023010
 Ajello, M., Angioni, R., Axelsson, M., et al. 2020, *ApJ*, 892, 105
 Ajello, M., Gasparrini, D., Sánchez-Conde, M., et al. 2015, *ApJ*, 800, L27
 Ajello, M., Romani, R. W., Gasparrini, D., et al. 2013, *ApJ*, 780, 73
 Ajello, M., Shaw, M. S., Romani, R. W., et al. 2012, *ApJ*, 751, 108
 Aloisio, R., Berezhinsky, V., & Blasi, P. 2014, *JCAP*, 2014, 020
 Alves Batista, R., Boncioli, D., di Matteo, A., van Vliet, A., & Walz, D. 2015, *JCAP*, 2015, 063
 Alves Batista, R., Dundovic, A., Erdmann, M., et al. 2016, *JCAP*, 2016, 038
 Atoyan, A., & Dermer, C. D. 2001, *PhRvL*, 87, 221102
 Banik, P., & Bhadra, A. 2019, *PhRvD*, 99, 103006
 Becker, J. K. 2008, *PhR*, 458, 173
 Berezhinskii, V. S., & Ginzburg, V. L. 1981, *MNRAS*, 194, 3
 Bhattacharya, A., Gandhi, R., Rodejohann, W., & Watanabe, A. 2011, *JCAP*, 10, 017
 Biehl, D., Fedynitch, A., Palladino, A., Weiler, T. J., & Winter, W. 2017, *JCAP*, 01, 033
 Böttcher, M., Reimer, A., Sweeney, K., & Prakash, A. 2013, *ApJ*, 768, 54
 Celotti, A., & Ghisellini, G. 2008, *MNRAS*, 385, 283
 Das, S., Gupta, N., & Razzaque, S. 2020, *ApJ*, 889, 149

- Dermer, C. D., & Menon, G. 2009, *High Energy Radiation from Black Holes: Gamma Rays, Cosmic Rays, and Neutrinos* (Princeton, NJ: Princeton Univ. Press)
- Eichler, D. 1979, *ApJ*, **232**, 106
- Fossati, G., Maraschi, L., Celotti, A., Comastri, A., & Ghisellini, G. 1998, *MNRAS*, **299**, 433
- Franckowiak, A., Garrappa, S., Paliya, V., et al. 2020a, *ApJ*, **893**, 162
- Franckowiak, A., et al. 2020b, *ApJ*, **893**, 162
- Gao, S., Fedynitch, A., Winter, W., & Pohl, M. 2019, *NatAs*, **3**, 88
- Garrappa, S., Buson, S., Franckowiak, A., et al. 2019, *ApJ*, **880**, 103
- Ghisellini, G., Righi, C., Costamante, L., & Tavecchio, F. 2017, *MNRAS*, **469**, 255
- Ghisellini, G., & Tavecchio, F. 2008, *MNRAS*, **387**, 1669
- Gilmore, R. C., Somerville, R. S., Primack, J. R., & Domínguez, A. 2012, *MNRAS*, **422**, 3189
- Giommi, P., Padovani, P., Oikonomou, F., et al. 2020, *A&A*, **640**, L4
- Heiter, C., Kuempel, D., Walz, D., & Erdmann, M. 2018, *Aph*, **102**, 39
- Huang, G.-y., & Liu, Q. 2020, *JCAP*, **03**, 005
- IceCube Collaboration, Aartsen, M., et al. 2013, *Sci*, **342**, 1242856
- IceCube Collaboration, Aartsen, M. G., Ackermann, M., et al. 2014, *PhRvL*, **113**, 101101
- IceCube Collaboration, Aartsen, M. G., Ackermann, M., et al. 2017a, *ApJ*, **849**, 67
- IceCube Collaboration, Aartsen, M. G., Ackermann, M., et al. 2017b, *Aph*, **92**, 30
- IceCube Collaboration, Aartsen, M. G., Abraham, K., et al. 2017c, *ApJ*, **835**, 45
- IceCube Collaboration, Aartsen, M. G., Ackermann, M., et al. 2018a, *Sci*, **361**, eaat1378
- IceCube Collaboration, Aartsen, M. G., Ackermann, M., et al. 2018b, *Sci*, **361**, 147
- Kalashev, O. E., Kusenko, A., & Essey, W. 2013, *PhRvL*, **111**, 041103
- KASCADE-Grande Collaboration, Apel, W. D., Arteaga-Velázquez, J. C., et al. 2011, *PhRvL*, **107**, 171104
- KASCADE-Grande Collaboration, Apel, W. D., Arteaga-Velázquez, J. C., et al. 2013, *PhRvD*, **87**, 081101
- Keivani, A., et al. 2018, *ApJ*, **864**, 84
- Kochocki, A., Takhistov, V., Kusenko, A., & Whitehorn, N. 2020, arXiv:2012.05955
- Lee, S. 1998, *PhRvD*, **58**, 043004
- Liu, R.-Y., Taylor, A. M., Wang, X.-Y., & Aharonian, F. A. 2016, *PhRvD*, **94**, 043008
- Mannheim, K., Stanev, T., & Biermann, P. L. 1992, *A&A*, **260**, L1
- Mastichiadis, A. 1996, *SSRv*, **75**, 317
- Mücke, A., Protheroe, R. J., Engel, R., Rachen, J. P., & Stanev, T. 2003, *Aph*, **18**, 593
- Murase, K., Dermer, C. D., Takami, H., & Migliori, G. 2012, *ApJ*, **749**, 63
- Murase, K., Inoue, Y., & Dermer, C. D. 2014, *PhRvD*, **90**, 023007
- Neronov, A., Semikoz, D., & Tchermin, C. 2014, *PhRvD*, **89**, 103002
- Padovani, P., Petropoulou, M., Giommi, P., & Resconi, E. 2015, *MNRAS*, **452**, 1877
- Palladino, A., Rodrigues, X., Gao, S., & Winter, W. 2019, *ApJ*, **871**, 41
- Petropoulou, M., Dimitrakoudis, S., Padovani, P., Mastichiadis, A., & Resconi, E. 2015, *MNRAS*, **448**, 2412
- Prince, R., Raman, G., Hahn, J., Gupta, N., & Majumdar, P. 2018, *ApJ*, **866**, 16
- Qu, Y., Zeng, H., & Yan, D. 2019, *MNRAS*, **490**, 758
- Razzaque, S. 2013, *PhRvD*, **88**, 081302
- Razzaque, S., Dermer, C. D., & Finke, J. D. 2012, *ApJ*, **745**, 196
- Rodrigues, X., Gao, S., Fedynitch, A., Palladino, A., & Winter, W. 2019, *ApJL*, **874**, L29
- Rodrigues, X., Heinze, J., Palladino, A., van Vliet, A., & Winter, W. 2020, arXiv:2003.08392
- Sahu, S., López Fortín, C. E., & Nagataki, S. 2019, *ApJL*, **884**, L17
- Sahu, S., & Zhang, B. 2018, *JHEAp*, **18**, 1
- Schneider, A. 2019, in 36th Int. Cosmic Ray Conf. 358 (Trieste: SISSA), 1004
- Sikora, M., Kirk, J. G., Begelman, M. C., & Schneider, P. 1987, *ApJL*, **320**, L81
- Stecker, F. W., Done, C., Salamon, M. H., & Sommers, P. 1991, *PhRvL*, **66**, 2697
- Steehgs, D., Mong, Y. L., Ramsay, G., et al. 2019, *GCN*, **25255**, 1
- Szabo, A., & Protheroe, R. 1994, *Aph*, **2**, 375
- Tavecchio, F. 2014, *MNRAS*, **438**, 3255
- Tavecchio, F., Ghisellini, G., & Guetta, D. 2014, *ApJ*, **793**, L18
- Taylor, A. M., Ahlers, M., & Hooper, D. 2015, *PhRvD*, **92**, 063011
- Taylor, A. M., Gabici, S., & Aharonian, F. 2014, *PhRvD*, **89**, 103003
- The Pierre Auger Collaboration, Aab, A., Abreu, P., et al. 2019, arXiv:1909.09073
- Xue, R., Liu, R.-Y., Petropoulou, M., et al. 2019, *ApJ*, **886**, 23
- Xue, R., Liu, R.-Y., Wang, X.-Y., Yan, H., & Böttcher, M. 2019, *ApJ*, **871**, 81
- Xue, R., Liu, R.-Y., Wang, Z.-R., Ding, N., & Wang, X.-Y. 2021, *ApJ*, **906**, 51
- Yuan, C., Murase, K., & Mészáros, P. 2020, *ApJ*, **890**, 25